molecular pharmaceutics

ARTICLE

pubs.acs.org/molecularpharmaceutics

^{64}Cu-Labeled Lissamine Rhodamine B: A Promising PET Radiotracer Targeting Tumor Mitochondria

Yang Zhou,[†] Young-Seung Kim,[†] Xin Yan,[†] Orit Jacobson,[‡] Xiaoyuan Chen,[‡] and Shuang Liu*[,†]

[†]School of Health Sciences, Purdue University, West Lafayette, Indiana, USA

[‡]Laboratory of Molecular Imaging and Nanomedicine (LOMIN), National Institute of Biomedical Imaging and Bioengineering (NIBIB), National Institutes of Health (NIH), Bethesda, Maryland, USA

Supporting Information

ABSTRACT: Enhanced mitochondrial potential in carcinoma cells is an important characteristic of cancer. It is of great current interest to develop a radiotracer that is sensitive to mitochondrial potential changes at the early stage of tumor growth. In this report, we present the synthesis and evaluation of ^{64}Cu-labeled Lissamine rhodamine B (LRB), ^{64}Cu(DOTA-LRB) (DOTA-LRB = 2-(6-(diethylamino)-3-(diethyliminio)-3*H*-xanthen-9-yl)-5-(*N*-(2-(2-(4,7,10-tris(carboxymethyl)-1,4,7,10-tetraazacyclododecan-1-yl)acetamido)ethyl)sulfamoyl)benzenesulfonate) as a new radiotracer for imaging tumors in athymic nude mice bearing U87MG human glioma xenografts by positron emission tomography (PET). We also explored its localization mechanism using Cu(DOTA-LRB) as the fluorescent probe in both the U87MG human glioma cell line and the cultured primary U87MG glioma cells. It was found that ^{64}Cu(DOTA-LRB) had the highest tumor uptake (6.54 ± 1.50, 6.91 ± 1.26, 5.68 ± 1.13, 7.58 ± 1.96, and 5.14 ± 1.50%ID/g at 0.5, 1, 2, 4, and 24 h postinjection, respectively) among many ^{64}Cu-labeled organic cations evaluated in the same animal model. The cellular staining study indicated that Cu(DOTA-LRB) was able to localize in mitochondria of U87MG glioma cells due to the enhanced negative mitochondrial potential. This statement is completely supported by the results from decoupling experiment with carbonylcyanide-*m*-chlorophenylhydrazone (CCCP). MicroPET data showed that the U87MG glioma tumors were clearly visualized as early as 30 min postinjection with ^{64}Cu(DOTA-LRB). ^{64}Cu(DOTA-LRB) remained stable during renal excretion, but underwent extensive degradation during hepatobiliary excretion. On the basis of the results from this study, it was concluded that ^{64}Cu(DOTA-LRB) represents a new class of promising PET radiotracers for noninvasive imaging of the MDR-negative tumors.

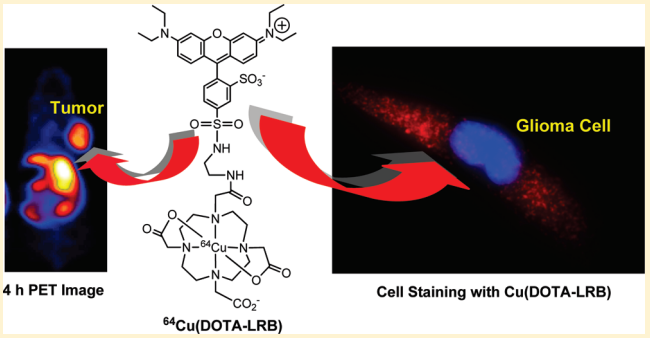

KEYWORDS: ^{64}Cu PET radiotracers, mitochondrial potential, tumor imaging

INTRODUCTION

Cancer is the second leading cause of death worldwide. The most prevalent forms of the disease are solid tumors of the lung, breast, prostate, colon and rectum.[1] Most cancer patients can survive for a long period of time after surgery, radiation and chemotherapy or a combination thereof if it can be detected at the early stage. Therefore, accurate early detection is highly desirable so that various therapeutic regimens can be given before the tumors become widely spread. Many imaging modalities are currently available for cancer detection. Ultrasonography (US), computed tomography (CT) and magnetic resonance imaging (MRI) can provide details of structural changes, variations in density and differences in proton content in tissues. However, significant challenges remain in using US, CT and MRI for molecular imaging of cancer. Nuclear medicine procedures using radiolabeled receptor ligands can provide the in vivo characterization of cellular structure and are able to monitor biological changes in the tumor tissues at the molecular level. A significant challenge for most of the receptor-based radiotracers is that not all the cancers or tumor tissues overexpress that specific receptor. Thus, it is of great benefit to develop a molecular imaging probe that could detect cancers by targeting a biomarker found in majority, if not all, of human cancer tissues.

Alteration in mitochondrial potential ($\Delta\Psi_m$) is characteristic of all human cancers.[2−5] It was reported that the mitochondrial potential in carcinoma cells is higher than that in normal cells of the surrounding tissues.[2−9] The observation that enhanced mitochondrial potential is prevalent in tumor cell phenotype provides the conceptual basis to develop the mitochondrion-targeted therapeutic pharmaceuticals and molecular imaging probes.[10−14] Since mitochondrial potential is negative, the delocalized organic cations tend to accumulate in the energized mitochondria of tumor cells.[15−18] For example, rhodamine derivatives have been widely used to determine the mitochondrial

Received: January 17, 2011
Accepted: May 5, 2011
Revised: April 29, 2011
Published: May 05, 2011

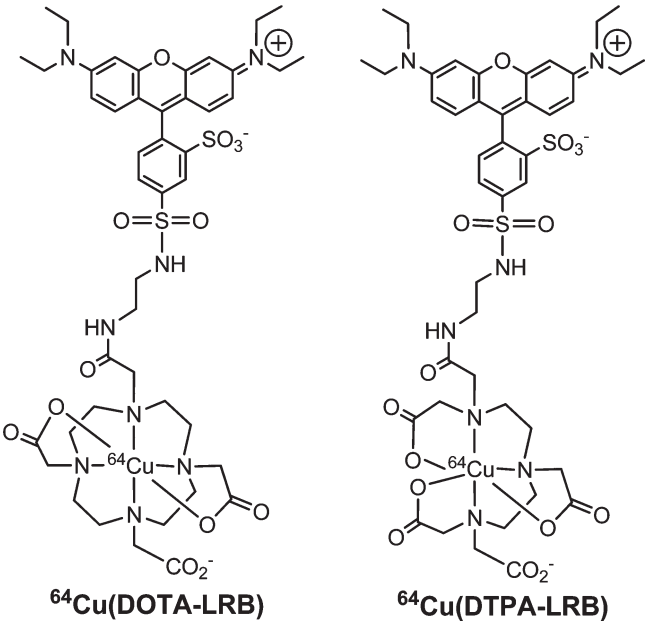

Figure 1. Proposed structures of ^{64}Cu(DOTA-LRB) and ^{64}Cu(DTPA-LRB). Lissamine rhodamine B (LRB) is used as the mitochondrion-targeting molecule to carry ^{64}Cu into tumor cells.

potential in tumor cells,[6−9] and as fluorescent probes for optical imaging of tumors.[19−25] Recently, Packard's group reported several ^{18}F-labeled rhodamine derivatives as PET (positron emission tomography) radiotracers for myocardial perfusion imaging.[26,27] Several research groups proposed to use the radiolabeled triphenylphosphonium (TPP) cations as PET radiotracers for both tumor and myocardial perfusion imaging.[28−37] It was reported that the tumor uptake of ^{3}H-tetraphenylphosphonium correlated well with tumor cell proliferation,[35] strongly suggesting that radiolabeled TPP cations might be useful for monitoring tumor aggressiveness. Even though biodistribution and imaging studies in small animals and dogs have demonstrated the utility of ^{11}C- and ^{18}F-labeled phosphonium cations for both heart and tumor imaging,[32−35,37] the combination of short half-life of ^{11}C ($T_{1/2}$ = 20.4 min) and ^{18}F ($T_{1/2}$ = 110 min) with their high background in normal organs (particularly heart and liver), poor availability and high cost makes the imaging with ^{11}C- and ^{18}F-labeled phosphonium cations impractical for routine clinic applications. Therefore, there is an urgent need for alternative PET radiotracers that detect the tumors at early stage by monitoring the mitochondrial potential difference between tumors and the surrounding normal tissues.

Lissamine rhodamine B (LRB) is a member of rhodamine derivatives, which have been widely utilized as fluorescent probes for determination of plasma and mitochondrial potentials,[6−9] and for optical imaging of tumors.[19−25] With this in mind, we prepared ^{64}Cu(DOTA-LRB) (Figure 1: DOTA-LRB = 2-(6-(diethylamino)-3-(diethyliminio)-3*H*-xanthen-9-yl)-5-(*N*-(2-(2-(4,7,10-tris(carboxymethyl)-1,4,7,10-tetraazacyclododecan-1-yl)acetamido)ethyl)sulfamoyl)benzenesulfonate). In ^{64}Cu-(DOTA-LRB), LRB is the mitochondrion-targeting biomolecule to carry ^{64}Cu into the tumor cells, where negative mitochondrial potential is elevated as compared with normal cells in the surrounding tissues. ^{64}Cu is a PET radionuclide with a β^+ emission (18%, E_{max} = 0.655 MeV) and has a half-life of 12.7 h. Even though its β^+ emission abundance is relatively low, the long half-life of ^{64}Cu makes it feasible to prepare, transport, and deliver the radiotracer for imaging applications. More importantly, recent breakthroughs in production of high specific-activity ^{64}Cu make it more available to small institutions without an on-site cyclotron.[38−44] ^{64}Cu is a viable alternative to ^{18}F for research programs that cannot afford to support and maintain the radionuclide production infrastructure. In addition, ^{64}Cu radiotracers will take full advantage of PET with respect to high sensitivity, high spatial resolution and ability to quantify radiotracer uptake. At the same time, they also enjoy the easy availability of kit formulation, if appropriately developed, for routine preparations in clinical settings.

In this report, we present the evaluation of ^{64}Cu(DOTA-LRB) as a new radiotracer for tumor imaging. Biodistribution and imaging studies were carried out in athymic nude mice bearing U87MG glioma xenografts, which express very little multidrug resistance P-glycoproteins (MDR Pgps) and multidrug resistance-associated proteins (MRPs).[45] Cu(DOTA-LRB) was prepared as the fluorescent probe for cellular staining assays to demonstrate its mitochondrial localization mechanism. For comparison purposes, we also prepared ^{64}Cu(DTPA-LRB) (Figure 1) to assess the impact of bifunctional chelators (BFCs) on biological properties of ^{64}Cu radiotracers.

EXPERIMENTAL SECTION

Materials and Instruments. Chemicals were purchased from Sigma/Aldrich (St. Louis, MO), and were used without further purification. Lissamine rhodamine B ethylenediamine (LRB) was purchased from AnaSpec Inc. (Fremont, CA). DOTA-(OBu-*t*)$_3$-NHS (1,4,7,10-tetraazacyclododecane-1,4,7-tris(*tert*-butyl acetate)-10-acetate mono(*N*-hydroxysuccinimide ester)) was purchased from Macrocyclics (Dallas, TX). The ESI (electrospray ionization) mass spectral data were collected on a Finnigan LCQ classic mass spectrometer, the School of Pharmacy, Purdue University. ^{64}Cu was produced using a CS-15 biomedical cyclotron at Washington University, School of Medicine by the ^{64}Ni(p,n)^{64}Cu nuclear reaction.

HPLC Methods. The semiprep HPLC method (method 1) used a LabAlliance HPLC system equipped with a UV/vis detector (λ = 254 nm) and Zorbax C_{18} semiprep column (9.4 nm × 250 mm, 100 Å pore size; Agilent Technologies, Santa Clara, CA). The flow rate was 2.5 mL/min, and the mobile phase was isocratic with 60% A (0.1% TFA in water) and 40% B (0.1% TFA in methanol) at 0−5 min, followed by a gradient mobile phase going from 40% B at 5 min to 100% B at 20 min. The radio-HPLC method (method 2) used the LabAlliance HPLC system equipped with a β-ram IN/US detector (Tampa, FL) and Vydac protein and peptide C_{18} column (4.6 mm × 250 mm, 300 Å pore size; Grace Davison Discovery Sciences, Hesperia, CA). The flow rate was 1 mL/min with the gradient mobile phase being isocratic with 90% solvent A (25 mM NH_4OAc, pH = 6.8) and 10% solvent B (acetonitrile) at 0−5 min, followed by a gradient mobile phase going from 10% B at 5 min to 90% B at 20 min. Method 3 used the LabAlliance HPLC system equipped with a UV/vis detector (λ = 254 nm), a β-ram IN-US detector, a Superose 12 10/300 GL size-exclusion column, and the flow rate of 0.4 mL/min. The aqueous mobile phase was isocratic with 20 mM HEPES and 150 mM NaCl.

2-(6-(Diethylamino)-3-(diethyliminio)-3*H*-xanthen-9-yl)-5-(*N*-(2-(2-(4,7,10-tris(carboxymethyl)-1,4,7,10-tetraazacyclododecan-1-yl)acetamido)ethyl)sulfamoyl)benzenesulfonate

(DOTA-LRB). DOTA(OBu-*t*)$_3$-NHS (5.4 mg, 6.6 μmol) and LRB-en (4.3 mg, 6 μmol) were dissolved in DMF (2 mL). To the mixture was added triethylamine (9 μL, 60 μmol). The mixture was stirred at room temperature overnight. Upon removal of volatiles under reduced pressure, the residue was dissolved in 2 mL of 12 N HCl. After the mixture was stirred at room temperature for 30 min, volatiles were removed under reduced pressure. The residue was dissolved in 2 mL of 50% DMF/water mixture, and the solution was subjected to HPLC purification (method 1). The fraction at 16 min was collected and lyophilized to give a purple powder (4.2 mg, 71%). ESI-MS: m/z = 987.10 for $[M + H]^+$ (986.4 calcd for $[C_{45}H_{62}N_8O_{13}S_2]^+$).

5-(*N*-(1-Carboxy-2,5,8-tris(carboxymethyl)-10-oxo-2,5,8,-11-tetraazatridecan-13-yl)sulfamoyl)-2-(6-(diethylamino)-3-(diethyliminio)-3*H*-xanthen-9-yl)benzenesulfonate (DTPA-LRB). To a solution of diethylenetriaminepentaacetic dianhydride (DTPA anhydride: 9.0 mg, 25 μmol) in a mixture of DMF (1 mL) and DMSO (0.5 mL) was added diisopropylethylamine (DIEA, 3 drops). To the mixture above was added LRB (1.8 mg, 2.5 μmol) in DMF (1 mL) dropwise over 1 h period. After addition of water (2 mL), the pH in the reaction mixture was adjusted to 4.0−5.0. The product was isolated by HPLC (method 1). Fractions at 16 min were collected and lyophilized to give a purple powder (0.9 mg, 37.5%). ESI-MS: m/z = 975.9 for $[M + H]^+$ (975.3 calcd for $[C_{43}H_{57}N_7O_{15}S_2]^+$).

Cu(DOTA-LRB). To a vial containing DOTA-LRB (6 mg, ~6 μmol) and $Cu(OAc)_2 \cdot H_2O$ (1.2 mg, 6 μmol) was added 1.5 mL of NH_4OAc (0.5 M, pH = 5.5). The resulting solution was heated at 100 °C for 30 min in a water bath. After the solution was cooled to room temperature, the product was isolated by HPLC (method 1). The fractions at 14.3 min were collected. Lyophilization of the collected fractions gave a purple powder (5.0 mg, 80%). ESI-MS: m/z = 1047.9 for $[M + H]^+$ (1047.3 calcd for $[C_{45}H_{60}CuN_8O_{13}S_2]^+$).

^{64}Cu-Labeling and Dose Preparation. To a clean Eppendorf tube was added 40 μg of DOTA-LRB dissolved in 0.3 mL of 0.1 M NaOAc buffer (pH = 6.5) and 20 μL of $^{64}CuCl_2$ solution (~500 μCi) in 0.05 N HCl. The reaction mixture was then heated at 100 °C for 20 min in a water bath. After heating, the vial was allowed to stand at room temperature for ~5 min. For ^{64}Cu(DTPA-LRB), radiolabeling could be completed by allowing the reaction mixture to stand at room temperature for 10−20 min. A sample of the resulting solution was analyzed by HPLC (method 2). Their log *P* values were determined according to the literature procedure.[46−48] For biodistribution studies, ^{64}Cu radiotracers were prepared and purified by HPLC. Volatiles in HPLC mobile phases were removed on a rotary evaporator. Doses were prepared by dissolving the purified ^{64}Cu radiotracer in saline to ~30 μCi/mL. The resulting solution was filtered with a 0.20 μm Millex-LG filter before being injected into animals. For the imaging study, ^{64}Cu(DOTA-LRB) was prepared and the resulting mixture was used without further purification.

Animal Model. Biodistribution studies were performed using the athymic nude mice bearing U87MG human glioma xenografts in compliance with the NIH animal experiment guidelines (*Principles of Laboratory Animal Care*, NIH Publication No. 86-23, revised 1985). The animal protocol was approved by the Purdue University Animal Care and Use Committee (PACUC). U87MG cells were cultured in minimum essential medium, Eagle with Earle's balanced salt solution (nonessential amino acids sodium pyruvate) (ATCC, Manassas, VA) in a humidified atmosphere of 5% CO_2, and were supplemented with 10% fetal bovine serum and 1% penicillin and streptomycin solution (GIBCO, Grand Island, NY). Female athymic nu/nu mice (5−6 weeks) were purchased from Harlan (Indianapolis, IN). Each mouse was implanted with 5×10^6 tumor cells subcutaneously into the left and right upper shoulder flanks. Four weeks after inoculation, the tumor size was 0.1−0.4 g, and animals were used for biodistribution studies.

Biodistribution Protocol. Twenty five tumor-bearing mice (20−25 g) were randomly divided into five groups. Each animal was administered with ~3 μCi of the ^{64}Cu radiotracer by tail vein injection. Five animals were sacrificed by sodium pentobarbital overdose (~200 mg/kg) at 0.5, 1, 2, 4, and 24 h p.i. Blood samples were withdrawn from the heart. The tumor, brain, eyes, heart, spleen, lungs, liver, kidneys, muscle and intestine were harvested, dried with absorbent tissue, weighed, and counted on a γ-counter (Perkin-Elmer Wizard-1480, Shelton, CT). The organ uptake was calculated as the percentage of injected dose per gram of organ mass (%ID/g) and the percentage of injected dose per organ (%ID/organ). Biodistribution data (%ID/g) and tumor-to-background (T/B) ratios are reported as an average plus the standard deviation based on the results from 5 tumor-bearing mice (10 tumors) at each time point. Comparison between different radiotracers was made using the two-way ANOVA test (GraphPad Prim 5.0, San Diego, CA). The level of significance was set at $p < 0.05$.

MicroPET. MicroPET scans were performed using an Inveon DPET scanner (Siemens Medical Solutions). The tumor-bearing nude mice (n = 3) were imaged in the prone position in the microPET scanner. Each mouse was injected with ~250 μCi of ^{64}Cu(DOTA-LRB) via the tail vein, then anesthetized with 2% isoflurane and placed near the center of FOV. Multiple 5 min static scans were obtained at 0.5, 1, 2, 4, and 24 h p.i. The images were reconstructed by a three-dimensional ordered subsets expectation maximum (3D-OSEM) algorithm. No correction was applied for attenuation or scatter. Image analysis was done using ASI Pro VM software.

Metabolic Stability. Normal athymic nude mice (n = 3) were used to study the metabolic stability of ^{64}Cu(DOTA-LRB). Each mouse was administered with ~100 μCi ^{64}Cu(DOTA-LRB) via tail vein. Urine samples were collected at 30 and 120 min p.i. by manual void, and were mixed with an equal volume of 50% acetonitrile aqueous solution. The mixture was centrifuged at 8,000 rpm. The supernatant was collected and passed through a 0.20 μm Millex-LG filter. The filtrate was analyzed by HPLC (method 2). Feces samples were collected at 120 min p.i. and suspended in 50% acetonitrile aqueous solution. The mixture was vortexed for 5−10 min. After centrifuging at 8,000 rpm, the supernatant was collected and passed through a 0.20 μm Millex-LG filter unit, and was then analyzed by HPLC (method 2). The radioactivity recovery was >90% for both urine and feces samples. The liver tissue was harvested at 120 min p.i., counted in a γ-counter, cut into small pieces, and then homogenized. The homogenate was mixed with 2 mL of 50% acetonitrile aqueous solution. The mixture was vortexed for 5−10 min. After centrifuging at 8000 rpm for 5 min, the supernatant was collected and counted in a γ-counter. The radioactivity recovery was ~35% from liver homogenate. After filtration through a 0.20 μm Milex-LG filter unit, the filtrate was then analyzed by HPLC (methods 2 and 3).

Cell Culture and Isolation Protocol. All the cell lines were purchased from American Type Culture Collection (ATCC, Manassas, VA). U87MG human glioma cells were cultured in the

Minimum Essential Medium supplemented with 10% fetal bovine serum (FBS, ATCC) and 1% penicillin and streptomycin (GIBCO) solution. Human fibroblasts were cultured in fibroblast dermal media supplemented with low serum growth kit (ATCC, including 7.5 mM L-glutamine, 5 ng/mL rh FGF β, 5 μg/mL insulin, 1 μg/mL hydrocortisone, 50 μg/mL ascorbic acid and 2% serum). The primary U87MG glioma tumor cells were extracted from xenografted U87MG tumors. Briefly, tumor tissues were cut and immersed immediately in completed Minimum Essential Medium (ATCC) media. The tumor tissues were rinsed twice with the Hanks solution and dissected into small pieces with razor blades. Small tumor pieces were digested with 0.25% trypsin (1 mM EDTA, without Ca^{2+} and Mg^{2+}) solution at 37 °C for 30 min, followed by vigorous pipetting and filtration through a 40 μm mesh nylon screen. After centrifugation at 1000 rpm for 5 min, the pellet was resuspended in the culture medium. All cells were grown at 37 °C in a humidified atmosphere containing 5% CO_2.

Cellular Staining Protocol. Cells (U87MG glioma and human fibroblasts cells) were allowed to culture in Lab-Tek 8-well glass chamber slides for at least 24 h before being used in the experiments. Cu(DOTA-LRB) was added into the cell culture medium to achieve a final concentration of 20 μM. Hoechst 33342 was added directly into the medium at a final concentration of 1 μM for 5 min before completion of incubation with Cu(DOTA-LRB). After incubation for 4 h, the tumor cells were washed three times with the phenol red-free Minimum Essential Medium. The fluorescence was visualized immediately with an Olympic BX51 fluorescence microscope (Olympus America Inc., Center Valley, PA) under 400× magnification.

Uncoupling Experiment. This experiment was carried out according to the literature methods[49,50] with slight modification using carbonyl cyanide *m*-chlorophenylhydrazone (CCCP) to disrupt the mitochondrial potential. In this experiment, U87MG glioma cells were pretreated with CCCP for 15 min. After incubation with Cu(DOTA-LRB) (20 μM) and CCCP (20, 50, 100 μM) for the specified time (0, 1, 4, and 8 h), U87MG glioma cells were washed with the phenol red-free Minimum Essential Medium. The fluorescence was visualized immediately with an Olympic BX51 fluorescence microscope. All images were acquired using a Hamamatsu digital CCD camera ORCA-R^2 (Hamamatsu Photonics K.K., Japan). Quantification of fluorescent intensity was performed using Olympus MetaMorph software (Molecular Devices, Sunnyvale, CA). The average of relative fluorescent intensity for each cell in each group was calculated from at least 15 randomly selected areas, and was normalized by the background fluorescence. Student's *t* test was used to determine the difference between CCCP-treated and control groups. The significant difference was set at $p < 0.05$.

RESULTS

DOTA-LRB and DTPA-LRB. DOTA-LRB was prepared by reacting LRB-en with DOTA(OBu-*t*)$_3$-NHS in DMF under basic conditions (pH: 8.5−9.0). Hydrolysis of the *tert*-butyl esters with concentrated HCl gave the expected product, which then was purified by HPLC. DTPA-LRB was prepared by direct conjugation of LRB-en with excess DTPA under similar conditions for DOTA-LRB. The chemical compositions of DOTA-LRB and DTPA-LRB were confirmed by ESI-MS data. Their HPLC purity was >95% before being used for radiolabeling.

Table 1. Radiochemical Purity (RCP), HPLC Retention Time and log *P* Values for ^{64}Cu Radiotracers

radiotracer	RCP (%)	retention time (min)	log *P* value
^{64}Cu(DOTA-LRB)	>95	14.6	-1.4 ± 0.1
^{64}Cu(DTPA-LRB)	>95	14.2	-1.5 ± 0.1
^{64}Cu(DO3A-xy-TPEP)	>95	13.7	-1.7 ± 0.1

Cu(DOTA-LRB). Cu(DOTA-LRB) was designed as a fluorescent probe for cellular staining experiments since it has identical chemical composition to that of ^{64}Cu(DOTA-LRB). It was prepared by reacting DOTA-LRB with one equivalent of Cu(II) acetate in 0.5 M NH_4OAc (pH = 5.5). HPLC concordance experiment showed that the retention times of Cu(DOTA-LRB) and ^{64}Cu(DOTA-LRB) were almost identical (14.3 min), suggesting that they have the same composition. The ESI-MS spectrum of Cu(DOTA-LRB) displays two molecular ions: m/z = 1047.9 for $[M + H]^+$ and m/z = 1070.0 for $[M + Na]^+$.

^{64}Cu(DOTA-LRB) and ^{64}Cu(DTPA-LRB). ^{64}Cu(DOTA-LRB) was prepared by reacting DOTA-LRB with $^{64}CuCl_2$ in 100 mM NH_4OAc buffer (pH = 5.0) at 100 °C for 10 min. ^{64}Cu(DTPA-LRB) could be readily prepared at room temperature. The radiochemical purity was >95% without HPLC purification with a specific activity of ~50 Ci/mmol. No further optimization was made to improve their specific activity. The HPLC retention times and log *P* values are listed in Table 1. ^{64}Cu(DOTA-LRB) (log $P = -1.4 \pm 0.1$) and ^{64}Cu(DTPA-LRB) (log $P = -1.5 \pm 0.1$) were more lipophilic than the ^{64}Cu-labeled phosphonium cations.[46−48] In addition, we found that ^{64}Cu(DOTA-LRB) was stable for >8 h after HPLC purification.

Biodistribution Characteristics. The biodistribution data for ^{64}Cu(DOTA-LRB) are listed in Table SI1 in the Supporting Information. Table SI2 in the Supporting Information summarizes the organ uptake and T/B ratios of ^{64}Cu(DTPA-LRB) at 4 h p.i. Figure 2 compares the selected organ uptake (%ID/g) and T/B ratios of ^{64}Cu(DOTA-LRB) and ^{64}Cu(DO3A-xy-TPEP) (DO3A-xy-TPEP = (2-(diphenylphosphoryl)ethyl)-diphenyl(4-((4,7,10-tris(carboxymethyl)-1,4,7,10-tetraazacyclododecan-1-yl)methyl)benzyl)phosphonium). ^{64}Cu(DO3A-xy-TPEP) was used for comparison since it has the best tumor uptake and T/B ratios among the ^{64}Cu-labeled phosphonium cations evaluated in the same glioma-bearing animal model.[46−48] We also obtained the biodistribution data (Table SI2 in the Supporting Information) for ^{64}Cu(DTPA-LRB) and $^{64}CuCl_2$. Figure 3 shows the selected organ uptake (%ID/g) and T/B ratios of ^{64}Cu(DOTA-LRB), ^{64}Cu(DTPA-LRB) and $^{64}CuCl_2$ at 4 h p.i. to illustrate the mitochondrion-targeting capability of LRB and the impact of BFC on biological properties of ^{64}Cu radiotracers.

In general, ^{64}Cu(DOTA-LRB) was excreted through the renal system with more than 65% of injected radioactivity being recovered from the urine sample at 1 h p.i. The blood radioactivity and tumor uptake of ^{64}Cu(DOTA-LRB) (Table SI1 in the Supporting Information) were significantly higher ($p < 0.01$) than those of ^{64}Cu(DO3A-xy-TPEP)[48] over 72 h. We were surprised that ^{64}Cu(DOTA-LRB) had tumor uptake (6.54 ± 1.50, 6.91 ± 1.26, 5.68 ± 1.13, 7.58 ± 1.96, and 5.14 ± 1.50% ID/g at 0.5, 1, 2, 4, and 24 h p.i., respectively) that is comparable to or higher than many radiolabeled multimeric cyclic RGD peptides evaluated in the glioma-bearing animal model.[52−56] The tumor uptake of ^{64}Cu(DOTA-LRB) remained almost

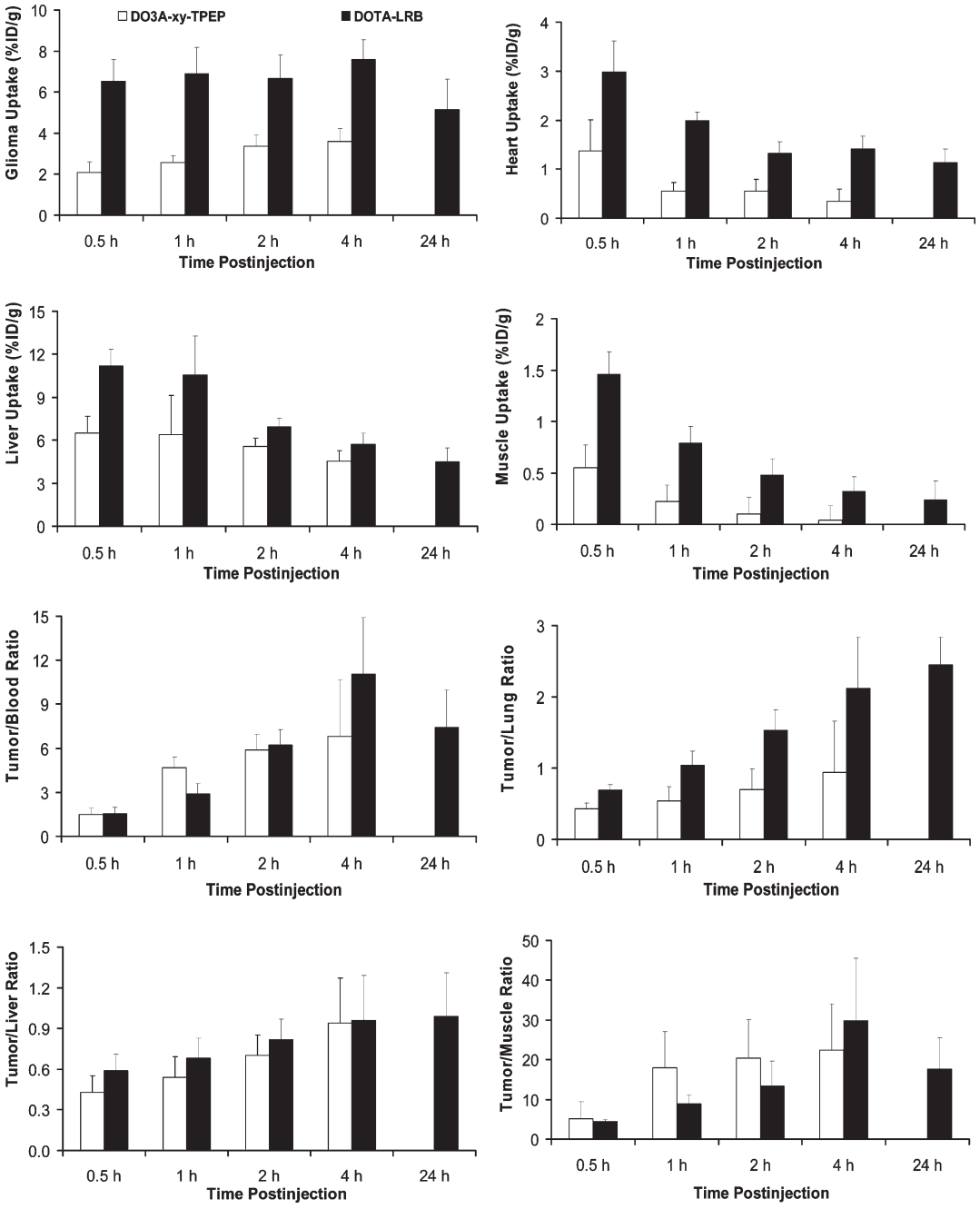

Figure 2. Direct comparison of the selected organ uptake and T/B ratios of ^{64}Cu(DOTA-LRB) and ^{64}Cu(DO3A-xy-TPEP) in the athymic nude mice (n = 5) bearing U87MG glioma xenografts.

unchanged while there was a slow increase in the tumor uptake of ^{64}Cu(DO3A-xy-TPEP) over the first 4 h. The uptake of ^{64}Cu-(DOTA-LRB) in the heart and muscle was also higher than that of ^{64}Cu(DO3A-xy-TPEP) during the same period. Tumor/liver ratios of ^{64}Cu(DOTA-LRB) were almost identical to those of ^{64}Cu(DO3A-xy-TPEP) over 4 h p.i. There were significant differences between ^{64}Cu(DOTA-LRB) and ^{64}Cu(DTPA-LRB). For example, the tumor uptake of ^{64}Cu(DOTA-LRB) was 7.6% ID/g (Figure 3) while it was 5.6%ID/g for ^{64}Cu(DTPA-LRB) at the same time point. ^{64}Cu(DOTA-LRB) had kidney uptake of 4.4%ID/g at 4 h p.i., which was 2× lower than that of ^{64}Cu-(DTPA-LRB) (8.9%ID/g at 4 h p.i.). The liver uptake (Table SI2 in the Supporting Information) was 7.7%ID/g for ^{64}Cu(DOTA-LRB) while the liver uptake was 31.3%ID/g for ^{64}Cu(DTPA-LRB) at the same time point. ^{64}Cu(DOTA-LRB) also showed a significantly lower blood radioactivity accumulation (0.7%ID/g at 4 h p.i.) than ^{64}Cu(DTPA-LRB) (2.7%ID/g at 4 h p.i.). Apparently, BFCs (DOTA vs DTPA) have a significant impact on the organ uptake and T/B ratios of ^{64}Cu radiotracers. Without the LRB targeting moiety, $^{64}CuCl_2$ had much lower tumor uptake (Figure 3) than ^{64}Cu(DOTA-LRB) and ^{64}Cu(DTPA-LRB). Thus, LRB is required for tumor localization of ^{64}Cu radiotracers. The uptake of $^{64}CuCl_2$ in normal organs (e.g., blood, heart, intestine, kidneys and liver) was well comparable

to that of ^{64}Cu(DTPA-LRB) within experimental error (Table SI2 in the Supporting Information).

MicroPET. Figure 4 shows microPET images of a glioma-bearing mouse administered with ~250 μCi of ^{64}Cu(DOTA-LRB) at 0.5, 1, 2, 4, and 24 h p.i. The tumor was clearly visualized as early as 30 min p.i. with excellent T/B contrast. No significant radioactivity accumulation was detected in the brain and muscle. After normalization, its tumor uptake values were 6.06 ± 0.07, 6.53 ± 0.48, 7.82 ± 1.06, 9.03 ± 0.95, and 4.75 ± 0.56%ID/g at 0.5, 1, 2, 4, and 24 h p.i., respectively. These data were completely consistent with those from biodistribution (Figure 2).

Metabolic Stability. Figure 5 shows radio-HPLC chromatograms of ^{64}Cu(DOTA-LRB) in saline before injection (A), in the urine at 30 min (B) and 120 min p.i. (C), and in the feces at 120 min p.i. (D). Apparently, it was stable during renal excretion over the 2 h period; but it underwent extensive degradation during hepatobiliary excretion as evidenced by the presence of two major radiometric peaks at 5 and 8 min (Figure 5D). We also examined its metabolic stability in liver. We found that ~35% of radioactivity was recovered from the liver homogenate. Using the reverse-phased column, there was one radiometric peak at 4 min (Figure 5E) with no intact ^{64}Cu(DOTA-LRB), suggesting that it underwent complete transchelation in the liver during the 2 h study period. Under the size-exclusion conditions, four radiometric peaks at 35, 40, 48, and 50 min were observed in the HPLC chromatogram (Figure 4F). The chromatographic patterns were almost identical to those reported for ^{64}Cu(DO3A-xy-TPEP) in nude mice,[48] and those for the ^{64}Cu-labeled tetraazamacrocycles in the rat liver.[56−58] Attempts to examine the stability of ^{64}Cu(DOTA-LRB) in the tumor were unsuccessful due to very low radioactivity recovery from the glioma tissues.

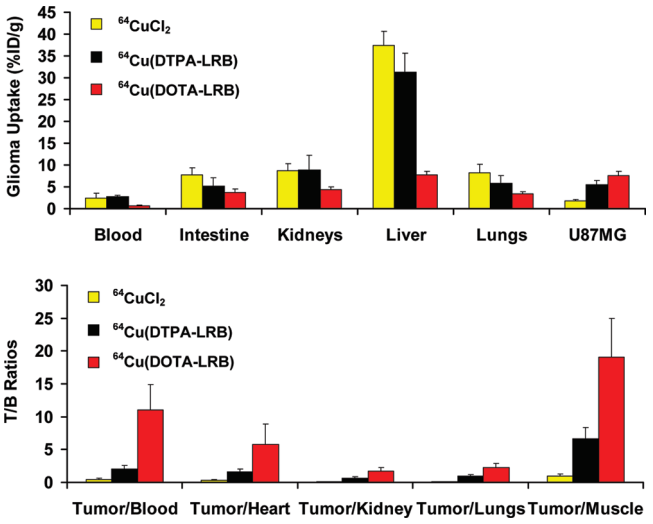

Figure 3. Direct comparison of the selected organ uptake and T/B ratios of ^{64}Cu(DOTA-LRB), ^{64}Cu(DTPA-LRB) and ^{64}CuCl$_2$ in athymic nude mice (n = 5) bearing U87MG glioma xenografts at 4 h p.i. These data clearly showed that the LRB moiety is required for tumor localization of ^{64}Cu radiotracers and BFC is important for their biodistribution characteristics.

Localization in Mitochondria. Figure 6 shows microscopic images of the primary U87MG glioma cells, U87MG human glioma cells and normal human fibroblast cells stained with 20 μM of Cu(DOTA-LRB). It was clear that Cu(DOTA-LRB) localize mainly in tumor mitochondria. It must be noted that Cu(DOTA-LRB) was also able to localize in the mitochondria of normal human fibroblast cells. However, the mitochondrial fluorescent intensity was too low to be seen clearly using the same brightness and contrast for the cultured primary U87MG glioma cells.

Differential Uptake and Mitochondrial Potential. An uncoupling experiment was used to demonstrate the importance of mitochondrial potential. In this experiment, CCCP was used to disrupt the mitochondrial potential in U87MG glioma cells. Figure 7 illustrates representative microscopic images of the U87MG glioma cells stained with 20 μM Cu(DOTA-LRB) with/without CCCP treatment, and the cellular fluorescent intensity quantification. It is quite clear that the fluorescence intensity in tumor mitochondria decreased dose-dependently after treatment with CCCP. At 100 μM, the relative fluorescent intensity is only about 1.2, which is close to the background. The uptake reduction of Cu(DOTA-LRB) in mitochondria of glioma cells was also time-dependent with the CCCP treatment (Figure SI1 in the Supporting Information).

DISCUSSION

Previously, we have evaluated a series of ^{64}Cu-labeled TPP and TPEP cations as potential PET radiotracers for imaging tumors in athymic nude mice bearing U87MG human glioma xenografts.[46−48] We found that ^{64}Cu(DO3A-xy-TPEP) has

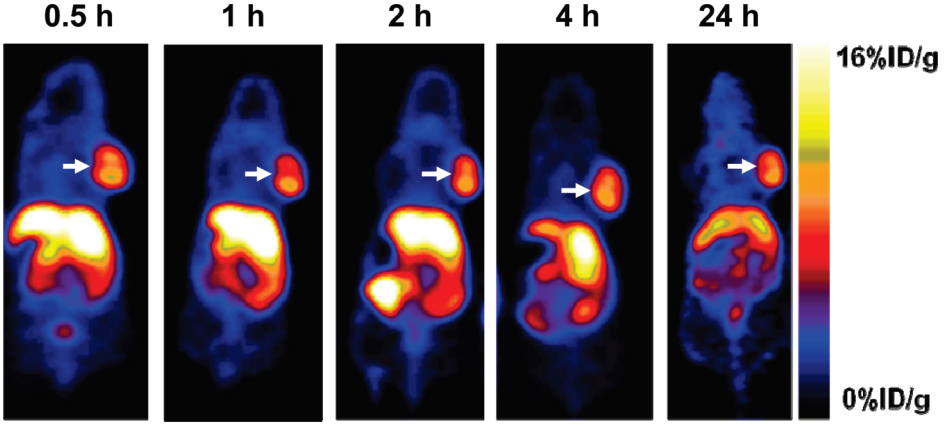

Figure 4. The decay-corrected whole-body coronal microPET images of the athymic nude mice bearing U87MG human glioma xenografts administered with ~250 μCi of ^{64}Cu(DOTA-LRB). Arrows indicate the presence of glioma tumors.

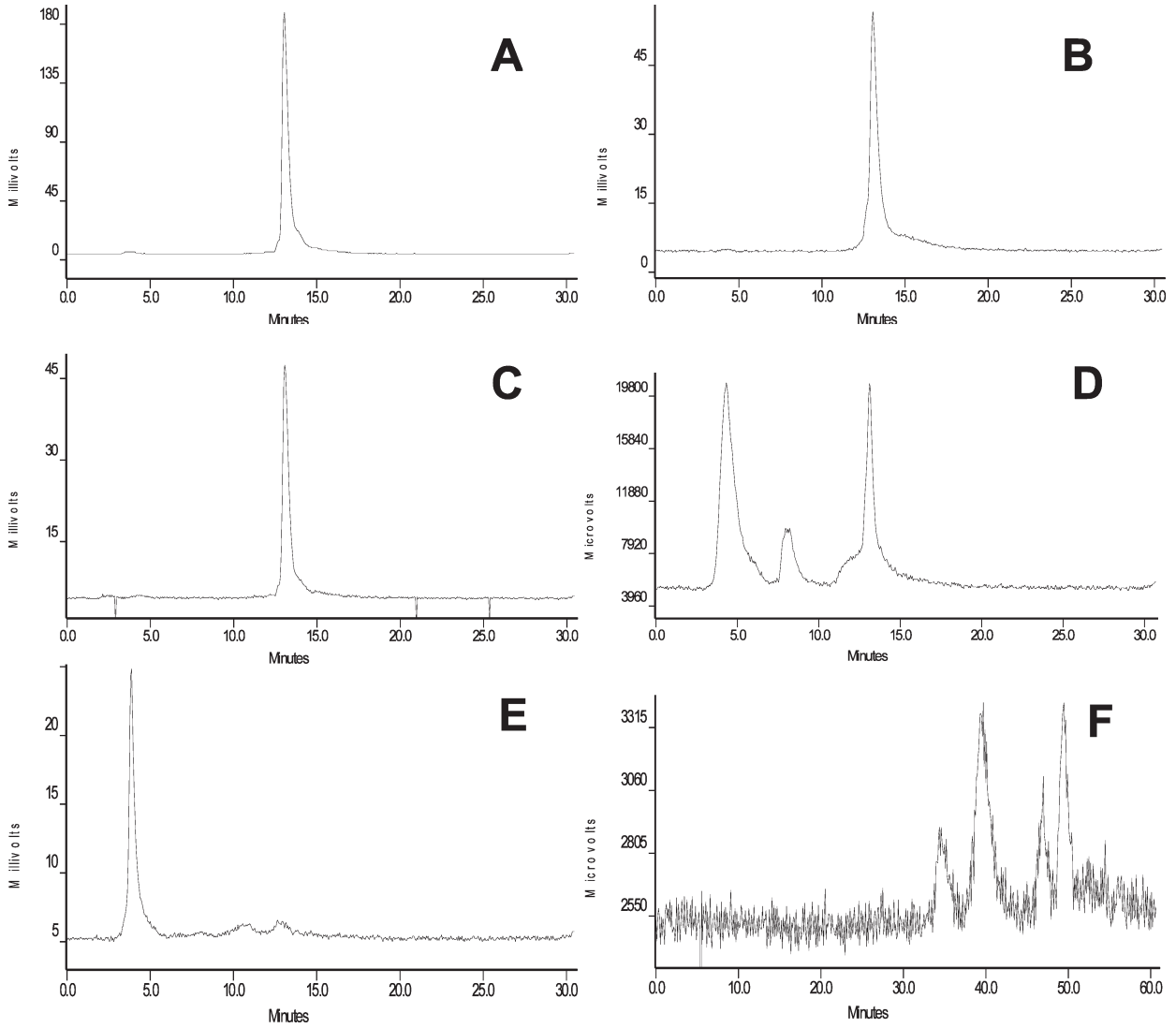

Figure 5. Representative radio-HPLC chromatograms of ^{64}Cu(DOTA-LRB) in saline before injection (A), in urine at 30 min (B) and 120 min p.i. (C), in feces at 120 min p.i. (D), and in the liver homogenate using the reverse-phased HPLC column (E) and the size-exclusion HPLC column (F).

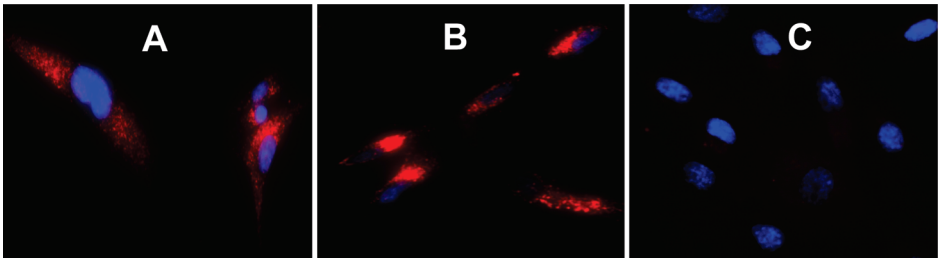

Figure 6. Representative microscopic images (magnification: 400×) of the cultured primary U87MG glioma cells (A), U87MG human glioma cells (B) and the normal human fibroblast cells (C) stained with 20 μM Cu(DOTA-LRB) (red color). The nuclei were stained with 1 μM Hoechst 33342 (blue color). Normal fibroblast cell line was used as the "negative control" to demonstrate the tumor selectivity of ^{64}Cu(DOTA-LRB).

higher tumor selectivity as compared to that of ^{99m}Tc-sestamibi.[48] In this study, we found that ^{64}Cu(DOTA-LRB) has significantly higher ($p < 0.01$) glioma uptake than that of ^{64}Cu(DO3A-xy-TPEP) over the 24 h study period (Figure 2). ^{64}Cu(DOTA-LRB) has the highest tumor uptake among the ^{64}Cu-labeled organic cations evaluated in the same glioma-bearing animal model.[46−48] The tumor/lung ratios of ^{64}Cu(DOTA-LRB) were better than those of ^{64}Cu(DO3A-xy-TPEP); but their tumor/liver ratios were comparable over 4 h p.i. On the basis of these results, we believe that ^{64}Cu(DOTA-LRB) is a better PET radiotracer than ^{64}Cu(DO3A-xy-TPEP) for imaging the MDR-negative tumors.

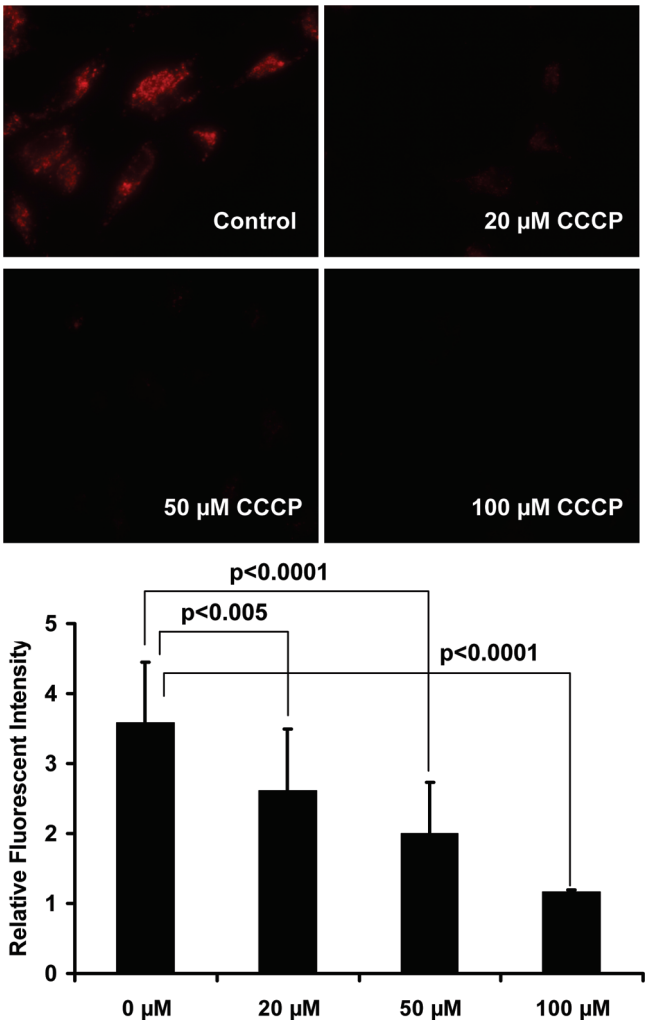

Figure 7. Representative microscopic images (magnification: 400×) of the living U87MG human glioma cells stained with 20 μM of Cu(DOTA-LRB)in the presence of CCCP (0, 20, 50, and 100 μM), and quantification of cellular fluorescent intensity. All images were adjusted with the same brightness and contrast. The relative fluorescent intensity for each cell in each group was calculated from at least 15 randomly selected areas, and was normalized by the background fluorescence.

It is unclear why ^{64}Cu(DOTA-LRB) has significantly higher ($p < 0.01$) tumor uptake than ^{64}Cu(DO3A-xy-TPEP) (Figure 2). On the basis of their lipophilicity (Table 1), one might suggest that the low tumor uptake is related to its lower lipophilicity and slower penetration kinetics across mitochondrial membrane. We believe that this explanation is oversimplified, given the fact other factors (e.g., the structure of targeting molecule, the coordination geometry of ^{64}Cu chelate and the overall molecular charge) will definitely have significant impact on biological properties of ^{64}Cu radiotracers. More studies are needed to further define the relationship between lipophilicity and tumor uptake kinetics of ^{64}Cu-labeled organic cations.

^{64}Cu(DOTA-LRB) undergoes extensive metabolic degradation (>65%) during hepatobiliary excretion (Figure 5). Similar metabolic instability was observed for ^{64}Cu(DOTA-xy-TPEP) (DOTA-xy-TPEP = (2-(diphenylphosphoryl)ethyl)diphenyl-(4-((2-(4,7,10-tris(carboxymethyl)-1,4,7,10-tetraazacyclododecan-1-yl)acetamido)methyl)benzyl)phosphonium).[48] We examined the liver stability of ^{64}Cu(DOTA-LRB), and found that no ^{64}Cu(DOTA-LRB) was intact in the extract from the liver homogenate (Figure 5). The HPLC profile (Figure 5F) of ^{64}Cu(DOTA-LRB) in the liver homogenate is very similar to those reported for ^{64}Cu(DO3A-xy-TPEP) in nude mice[48] and the ^{64}Cu-labeled tetraazamacrocycles in the rat liver homogenate using the same size-exclusion method.[56−58] Therefore, we believe that the four radiometric peaks (Figure 5F) are likely caused by complete transchelation of ^{64}Cu from ^{64}Cu(DOTA-LRB) to the proteins, such as superoxide dismutase, abundant in the liver. This statement is further supported by the fact that ^{64}Cu(DTPA-LRB) is unstable in vivo, and has liver uptake (Table SI2 in the Supporting Information) ∼4× higher than that of ^{64}Cu(DOTA-LRB). The fact that ^{64}Cu(DTPA-LRB) and ^{64}CuCl$_2$ share similar uptake in normal organs, such as blood, heart, intestine, kidneys and liver (Table SI2 in the Supporting Information), strongly suggests that the high uptake of ^{64}Cu(DTPA-LRB) in these organs is caused by the in vivo instability of the ^{64}Cu(DTPA) chelate.

The mitochondrial localization of ^{64}Cu(DOTA-LRB) has been clearly demonstrated using Cu(DOTA-LRB) as the fluorescent probe (Figure 6A,B). Since Cu(DOTA-LRB) is also able to localize in human fibroblasts (Figure 6C), the difference in fluorescent intensity inside the mitochondria is most likely originated from the increased mitochondrial potential in U87MG glioma cells as compared with that of normal fibroblasts. This statement is completely supported by the results from decoupling experiment with CCCP (Figure 7). These results strongly support our hypothesis that the tumor selectivity of ^{64}Cu(DOTA-LRB) is caused by the increased negative mitochondrial potential in U87MG glioma cells as compared to the cells from surrounding normal tissues.

We have been intrigued by the mitochondrion-targeting capability of LRB. As demonstrated in this study, ^{64}Cu(DOTA-LRB) can localize in tumor mitochondria with a long tumor retention time. Biodistribution data (Tables SI1 and SI2 in the Supporting Information) showed that ^{64}Cu(DTPA-LRB) and ^{64}CuCl$_2$ share similar uptake in normal organs (Table SI2 in the Supporting Information), such as blood, heart, intestine, kidneys and liver due to in vivo instability of ^{64}Cu(DTPA-LRB). The dramatic difference in their glioma uptake (^{64}Cu(DTPA-LRB), 5.6%ID/g; and ^{64}CuCl$_2$, 1.8%ID/g) strongly suggests that the LRB moiety is needed for ^{64}Cu(DTPA-LRB) and ^{64}Cu(DOTA-LRB) to selectively target the energized mitochondria of tumor cells and to achieve a high uptake in tumor tissues. We also made many attempts to examine the stability of ^{64}Cu(DOTA-LRB) in tumor tissues without success due to very low radioactivity recovery. The fact that the radioactivity recovered from tumor tissues was too low for HPLC analysis seems to suggest that ^{64}Cu(DOTA-LRB) might be decomposed as it is in the liver (Figure 5) once it is taken into the tumor mitochondria. From this point of view, the long tumor retention is probably caused by its instability in tumor mitochondria. This statement is further supported by the fact that ^{64}Cu(DTPA-LRB) has very low stability, and its tumor uptake (Table SI2 in the Supporting Information) is close to that of ^{64}Cu(DOTA-LRB) since they both are able to release a certain amount of ^{64}Cu into the tumor cells. It seems that there is always a balance between the in vivo stability of the ^{64}Cu-BFC chelate and the tumor uptake of ^{64}Cu radiotracers. If the ^{64}Cu-BFC chelate is too unstable in vivo, the ^{64}Cu radiotracer may become completely decomposed to release ^{64}Cu, which will definitely result in high liver uptake. The next question is how stable is enough for the ^{64}Cu-BFC chelate. More

studies are required to further define the relationship between the in vivo stability of ^{64}Cu-BFC chelates on the tumor uptake and retention time of ^{64}Cu-labeled rhodamine derivatives.

One might be concerned that ^{64}Cu(DOTA-LRB) has little usage for glioma imaging in clinics due to its poor brain penetration capability. As a matter of fact, this is its significant advantage since ^{64}Cu(DOTA-LRB) has very low radioactivity accumulation in normal tissues of the brain (Figure 2). Since tumors have more leaky capillaries, the blood brain barrier is not a significant issue for ^{64}Cu-labeled rhodamine cations. ^{99m}Tc-sestamibi and ^{99m}Tc-tetrofosmin are cationic, and have been used for imaging brain tumors in cancer patients.[59−61] ^{11}C-TPP is also cationic, and was used to image brain tumors in dogs.[32]

CONCLUSION

In summary, we evaluated ^{64}Cu(DOTA-LRB) as a new PET radiotracer to image tumors in athymic nude mice bearing U87MG human glioma xenografts. We found that ^{64}Cu-(DOTA-LRB) has the highest tumor uptake among ^{64}Cu-labeled organic cations evaluated in the glioma-bearing model. It is surprising that a simple molecule like ^{64}Cu(DOTA-LRB) could have tumor uptake higher than or comparable to that of many radiolabeled multimeric cyclic RGD peptides in the same animal model.[51−55] We also explored its localization mechanism in U87MG glioma cells, and found that Cu(DOTA-LRB) is able to selectively localize in the tumor mitochondria. Its long tumor retention time is probably caused by its intracellular instability. On the basis of these results, we believe that ^{64}Cu(DOTA-LRB) is a promising lead compound for the development of mitochondrion-directed ^{64}Cu PET radiotracers, but further minimization of liver uptake is needed. In addition, Cu(DOTA-LRB) is also an excellent fluorescent probe, which makes the dual modality imaging (PET and optical) possible using two imaging agents, ^{64}Cu(DOTA-LRB) and Cu(DOTA-LRB), with the same composition. In this way, we are able to demonstrate the tumor localization of the ^{64}Cu radiotracer by PET, and at the same time we can visualize its intracellular location in living tumor cells by fluorescent assays or optical imaging methods.

ASSOCIATED CONTENT

Supporting Information. Selected biodistribution data for ^{64}Cu(DOTA-LRB) (Table SI1), ^{64}Cu(DTPA-LRB) (Table SI2) and $^{64}CuCl_2$ (Table SI2) in athymic nude mice bearing U87MG human glioma xenografts, and representative microscopic images (Figure SI1) of the living U87MG glioma cells stained with 50 μM of Cu(DOTA-LRB) in the presence of 50 μM CCCP for 0, 1, 4, and 8 h. This material is available free of charge via the Internet at http://pubs.acs.org.

AUTHOR INFORMATION

Corresponding Author

*School of Health Sciences, Purdue University, 550 Stadium Mall Drive, West Lafayette, IN 47907. Phone: 765-494-0236. Fax: 765-496-1377. E-mail: liu100@purdue.edu.

ACKNOWLEDGMENT

This work is supported, in part, by Purdue University and Research Grant R01 CA115883 from the National Cancer Institute (NCI).

REFERENCES

(1) Jemal, A.; Siegel, R.; Xu, J.; Ward, E. Cancer statistics, 2010. *Ca-Cancer J. Clin.* **2010**, *60*, 1–24.

(2) Kroemer, G.; Dallaporta, B.; Resche-Rigon, M. The mitochondrial death/life regulator in apoptosis and necrosis. *Annu. Rev. Physiol.* **1998**, *60*, 619–642.

(3) Modica-Napolitano, J. S.; Aprille, J. R. Delocalized lipophilic cations selectively target the mitochondria of carcinoma Cells. *Adv. Drug Delivery Rev.* **2001**, *49*, 63–70.

(4) Duchen, M. R. Mitochondria in health and disease: perspectives on a new mitochondrial biology. *Mol. Aspects Med.* **2004**, *25*, 365–451.

(5) Mannella, C. A. The relevance of mitochondrial membrane topology to mitochondrial function. *Biochim. Biophys. Acta* **2006**, *1762*, 140–147.

(6) Summerhayes, I. C.; Lampidis, T. J.; Bernal, S. D.; Nadakavukaren, J. J.; Nadakavukaren, K. K.; Shepard, E. L.; Chen, L. B. Unusual retention of Rhodamine 123 by mitochondria in muscle and carcinoma cells. *Proc. Natl. Acad. Sci. U.S.A.* **1982**, *77*, 990–994.

(7) Modica-Napolitano, J. S.; Aprille, J. R. Basis for the selective cytotoxicity of Rhodamine 123. *Cancer Res.* **1987**, *47*, 4361–4365.

(8) Davis, S.; Weiss, M. J.; Wong, J. R.; Lampidis, T. J.; Chen, L. B. Mitochondrial and plasma membrane potentials cause unusual accumulation and retention of Rhodamine 123 by human breast adenocarcinoma-derived MCF-7 cells. *J. Biol. Chem.* **1985**, *260*, 13844–13850.

(9) Dairkee, S. H.; Hackett, A. J. Differential retention of Rhodamine 123 by breast carcinoma and normal human mammary tissue. *Breast Cancer Res. Treat.* **1991**, *18*, 57–61.

(10) Modica-Napolitano, J. S.; Singh, K. K. Mitochondria as targets for detection and treatment of Cancer. *Expert Rev. Mol. Med.* **2002**, *4*, 1–19.

(11) Gottlieb, E.; Thompson, C. B. Targeting the mitochondria to enhance tumor suppression. *Methods Mol. Biol.* **2003**, *223*, 543–554.

(12) Ross, M. F.; Kelso, G. F.; Blaikie, F. H.; James, A. M.; Cocheme, H. M.; Filipovska, A.; Da Ros, T.; Hurd, T. R.; Smith, R. A.; Murphy, M. P. Lipophilic triphenylphosphonium cations as tools in mitochondrial bioenergetics and free radical biology. *Biochemistry (Moscow)* **2005**, *70*, 222–230.

(13) Licha, K.; Olbrich, C. Optical imaging in drug discovery and diagnostic applications. *Adv. Drug Delivery Rev.* **2005**, *57*, 1087–1108.

(14) Jakobs, S. High resolution imaging of live mitochondria. *Biochim. Biophys. Acta* **2006**, *1763*, 561–575.

(15) Lichtshtein, D.; Kaback, H. R.; Blume, A. J. Use of a lipophilic cation for determination of membrane potential in neuroblastoma-glioma hybrid cell suspensions. *Proc. Natl. Acad. Sci. U.S.A.* **1979**, *76*, 650–654.

(16) Hockings, P. D.; Rogers, P. J. The Measurement of transmembrane electrical potential with lipophilic cations. *Biochim. Biophys. Acta* **1996**, *1282*, 101–106.

(17) Huang, S. G. Development of a high throughput screening assay for mitochondrial membrane potential in living cells. *J. Biomol. Screening* **2002**, *7*, 383–389.

(18) Lefevre, C.; Kang, H. C.; Haugland, R. P.; Malekzadeh, N.; Arttamangkul, S.; Haugland, R. P. Texas Red-X and Rhodamine Red-X, new derivatives of sulforhodamine 101 and Lissamine Rhodamine B with improved labeling and fluorescence properties. *Bioconjugate Chem.* **1996**, *7*, 482–489.

(19) Lavis, L. D; Chao, T. Y.; Raines, R. T. Fluorogenic label for biomolecular imaging. *ACS Chem. Biol.* **2006**, *1*, 252–260.

(20) Mao, C.; Kisaalita, W. S. Determination of resting membrane potential of individual neuroblastoma cells (IMR-32) using a potentiometric dye (TMRM) and confocal microscopy. *J. Fluoresc.* **2004**, *14*, 739–743.

(21) Scaduto, R. C., Jr.; Grotyohann, L. W. Measurement of mitochondrial membrane potential using fluorescent rhodamine derivatives. *Biophys. J.* **1999**, *76*, 469–477.

(22) Hama, Y.; Urano, Y.; Koyama, Y.; Kamiya, M.; Bernardo, M.; Paik, R. S.; Shin, I. S.; Paik, C. H.; Choyke, P. L.; Kobayashi, H. A target

cell-specific activatable fluorescence probe for *in vivo* molecular imaging of cancer based on a self-quenched Avidin-Rhodamine conjugate. *Cancer Res.* **2007**, *67*, 2791–2799.

(23) Glunde, K.; Foss, C. A.; Takagi, T.; Wildes, F.; Bhujwalla, Z. M. Synthesis of 6′-*O*-Lissamine-Rhodamine B-glucosamine as a novel probe for fluorescence imaging of lysosomes in breast tumors. *Bioconjugate Chem.* **2005**, *16*, 843–851.

(24) Longmire, M. R.; Ogawa, M.; Hama, Y.; Kosaka, N.; Regino, C. A.; Choyke, P. L.; Kobayashi, H. Determination of optimal rhodamine fluorophore for *in vivo* optical imaging. *Bioconjugate Chem.* **2008**, *19*, 1735–1742.

(25) Yova, D.; Atlamazoglou, V.; Kavantzas, N.; Loukas, S. Development of a fluorescence-based imaging system for colon cancer diagnosis using two novel rhodamine derivatives. *Lasers Med. Sci.* **2000**, *15*, 140–147.

(26) Heinrich, T. K.; Gottumukkala, V.; Snay, E.; Dunning, P.; Fahey, F. H.; Ted Treves, S.; Packard, A. B. Synthesis of fluorine-18 labeled Rhodamine B: a potential PET myocardial perfusion imaging agent. *Appl. Radiat. Isot.* **2010**, *68*, 96–100.

(27) Gottumukkala, V.; Heinrich, T. K.; Baker, A.; Dunning, P.; Fahey, F. H.; Treves, S. T.; Packard, A. B. Biodistribution and stability studies of [^{18}F]fluoroethylrhodamine B, a potential PET myocardial perfusion agent. *Nucl. Med. Biol.* **2010**, *37*, 365–370.

(28) Srivastava, P. C.; Knapp, F. F., Jr. [(*E*)-1-[^{123}I]Iodo-1-penten-5-Yl]triphenylphosphonium iodide: convenient preparation of a potentially useful myocardial perfusion agent. *J. Med. Chem.* **1984**, *27*, 978–981.

(29) Srivastava, P. C.; Hay, H. G.; Knapp, F. F., Jr. Effects of alkyl and aryl substitution on the myocardial specificity of radioiodinated phosphonium, arsonium, and ammonium cations. *J. Med. Chem.* **1985**, *28*, 901–904.

(30) Steichen, J. D.; Weiss, M. J.; Elmaleh, D. R.; Martuza, R. L. Enhanced *in vitro* uptake and retention of ^{3}H-tetraphenylphosphonium by nerve system tumor cells. *J. Neurosurg.* **1991**, *74*, 116–122.

(31) Krause, B. J.; Szabo, Z.; Becker, L. C.; Dannals, R. F.; Scheffel, U.; Seki, C.; Ravert, H. T.; Dipaola, A. F., Jr.; Wagner, H. N., Jr. Myocardial perfusion with [^{11}C] methyl triphenyl phosphonium: measurements of the extraction fraction and myocardial uptake. *J. Nucl. Biol. Med.* **1994**, *38*, 521–526.

(32) Madar, I.; Anderson, J. H.; Szabo, Z.; Scheffel, U.; Kao, P. F.; Ravert, H. T.; Dannals, R. F. Enhanced uptake of [^{11}C]TPMP in canine brain tumor: a PET study. *J. Nucl. Med.* **1999**, *40*, 1180–1185.

(33) Madar, I.; Weiss, L.; Izbicki, G. Preferential accumulation of ^{3}H-tetraphenylphosphonium in non-small cell lung carcinoma in mice: comparison with ^{99m}Tc-MIBI. *J. Nucl. Med.* **2002**, *43*, 234–238.

(34) Madar, I.; Ravert, H. T.; Du, Y.; Hilton, J.; Volokh, L.; Dannals, R. F.; Frost, J. J.; Hare, J. M. Characterization of uptake of the new PET imaging compound [^{18}F]fluorobenzyl triphenylphosphonium in dog myocardium. *J. Nucl. Med.* **2006**, *47*, 1359–1366.

(35) Min, J. J.; Biswal, S.; Deroose, C.; Gambhir, S. S. Tetraphenylphosphonium as a novel molecular probe for imaging tumors. *J. Nucl. Med.* **2004**, *45*, 636–643.

(36) Cheng, Z.; Winant, R. C.; Gambhir, S. S. A new strategy to screen molecular imaging probe uptake in cell culture without radiolabeling using matrix-assisted laser desorption/ionization time-of-flight mass spectrometry. *J. Nucl. Med.* **2005**, *46*, 878–886.

(37) Shoup, T. M.; Elmaleh, D. R.; Brownell, A. L.; Zhu, A.; Guerrero, J. L.; Fischman, A. J. Evaluation of (4-[^{18}F]fluorophenyl)-triphenylphosphonium ion. A potential myocardial blood flow agent for PET. *Mol. Imaging Biol.* **2010**, available online.

(38) Anderson, C. J.; Green, M. A.; Fujibayashi, Y. Chemistry of copper radionuclides and radiopharmaceutical products. In *Handbook of Radiopharmaceuticals: Radiochemistry and Applications*; Welch, M. J., Redvanly, C., Eds.; John Wiley & Sons, Ltd.: 2003; pp 401−422.

(39) Blower, P. J.; Lewis, J. S.; Zweit, J. Copper radionuclides and radiopharmaceuticals in nuclear medicine. *Nucl. Med. Biol.* **1996**, *23*, 957–980.

(40) Smith, S. V. Molecular imaging with copper-64. *J. Inorg. Biochem.* **2004**, *98*, 1874–1901.

(41) Liu, S. The role of coordination chemistry in the development of target-specific radiopharmaceuticals. *Chem. Soc. Rev.* **2004**, *33*, 445–461.

(42) Reichert, D. E.; Lewis, J. S.; Anderson, C. J. Metal complexes as diagnostic tools. *Coord. Chem. Rev.* **1999**, *184*, 3–66.

(43) Anderson, C. J.; Welch, M. J. Radiometal-labeled agents (Non-Technetium) for diagnostic imaging. *Chem. Rev.* **1999**, *99*, 2219–2234.

(44) Liu, S. Bifunctional coupling agents for radiolabeling of biomolecules and target-specific delivery of metallic radionuclides. *Adv. Drug Delivery Rev.* **2008**, *60*, 1347–1370.

(45) Liu, S.; Kim, Y. S.; Zhai, S.; Shi, J.; Hou, G. Evaluation of ^{64}Cu(DO3A-xy-TPEP) as a potential PET radiotracer for monitoring tumor multidrug resistance. *Bioconjugate Chem.* **2009**, *20*, 790–798.

(46) Wang, J.; Yang, C. T.; Kim, Y. S.; Sreerama, S. G.; Cao, Q.; Li, Z. B.; He, Z.; Chen, X.; Liu, S. ^{64}Cu-Labeled triphenylphosphonium and triphenylarsonium cations as highly tumor-selective imaging agents. *J. Med. Chem.* **2007**, *50*, 5057–5069.

(47) Kim, Y. S.; Yang, C.; Wang, J.; Sreerama, S. G.; Cao, Q.; Li, Z.; He, Z.; Chen, X.; Liu, S. Effects of targeting moiety, linker, bifunctional chelator, and molecular charge on biological properties of ^{64}Cu-labeled triphenylphosphonium cations. *J. Med. Chem.* **2008**, *51*, 2971–2984.

(48) Yang, C. T.; Kim, Y. S.; Wang, J.; Wang, L.; Shi, J.; Li, Z. B.; Chen, X.; Fan, M.; Li, J. J.; Liu, S. ^{64}Cu-Labeled 2-(diphenylphosphoryl)-ethyldiphenylphosphonium cations as highly selective tumor imaging agents: effects of linkers and chelates on radiotracer biodistribution characteristics. *Bioconjugate Chem.* **2008**, *19*, 2008–2022.

(49) de Graaf, A. O.; van den Heuvel, L. P.; Dijkman, H. B.; de Abreu, R. A.; Birkenkamp, K. U.; de Witte, T.; van der Reijden, B. A.; Smeitink, J. A.; Jansen, J. H. Bcl-2 prevents loss of mitochondria in CCCP-induced apoptosis. *Exp. Cell Res.* **2004**, *299*, 533–540.

(50) Horton, K. L.; Stewart, K. M.; Fonseca, S. B.; Guo, Q.; Kelley, S. O. Mitochondria-penetrating peptides. *Chem. Biol.* **2008**, *15*, 375–382.

(51) Chen, X.; Liu, S.; Hou, Y.; Tohme, M.; Park, R.; Bading, J. R.; Conti, P. S. MicroPET imaging of breast cancer α_v-integrin expression with ^{64}Cu-labeled dimeric RGD-peptides. *Mol. Imaging Biol.* **2004**, *6*, 350–359.

(52) Wu, Y.; Zhang, X.; Xiong, Z.; Cheng, Z.; Fisher, D. R.; Liu, S.; Gambhir, S. S.; Chen, X. MicroPET imaging of glioma integrin $\alpha_v\beta_3$ expression using ^{64}Cu-labeled tetrameric RGD peptide. *J. Nucl. Med.* **2005**, *46*, 1707–1718.

(53) Shi, J.; Kim, Y. S.; Zhai, S.; Liu, Z.; Chen, X.; Liu, S. Improving tumor uptake and pharmacokinetics of ^{64}Cu-labeled cyclic RGD peptide dimers with Gly_3 and PEG_4 linkers. *Bioconjugate Chem.* **2009**, *20*, 750–759.

(54) Wang, L.; Shi, J.; Kim, Y. S.; Zhai, S.; Jia, B.; Zhao, H.; Liu, Z.; Wang, F.; Chen, X.; Liu, S. Improving tumor-targeting capability and pharmacokinetics of ^{99m}Tc-labeled cyclic RGD dimers with PEG_4 linkers. *Mol. Pharmaceutics* **2009**, *6*, 231–245.

(55) Shi, J.; Wang, L.; Kim, Y. S.; Zhai, S.; Liu, Z.; Chen, X.; Liu, S. Improving tumor uptake and excretion kinetics of ^{99m}Tc-labeled cyclic Arginine-Glycine-Aspartic (RGD) dimers with triglycine linkers. *J. Med. Chem.* **2008**, *51*, 7980–7990.

(56) Boswell, C. A.; Sun, X.; Niu, W.; Weisman, G. R.; Wong, E. H.; Rheingold, A. L.; Anderson, C. J. Comparative in vivo stability of copper-64-labeled cross-bridged and conventional tetraazamacrocyclic complexes. *J. Med. Chem.* **2004**, *47*, 1465–1474.

(57) Boswell, C. A.; McQuade, P.; Weisman, G. R.; Wong, E. H.; Anderson, C. J. Optimization of labeling and metabolite analysis of copper-64-labeled azamacrocyclic chelators by radio-LC-MS. *Nucl. Med. Biol.* **2005**, *32*, 29–38.

(58) Sprague, J. E.; Peng, Y.; Fiamengo, A. L.; Woodin, K. S.; Southwick, E. A.; Wiseman, G. R.; Wong, E. H.; Golden, J. A.; Rheingold, A. L.; Anderson, C. J. Synthesis, characterization and in vivo studies of Cu(II)-64-labeled cross-bridged tetraazamacrocycle-amide complexes as models of peptide conjugate imaging agents. *J. Med. Chem.* **2007**, *50*, 2527–2535.

(59) Choi, J. Y.; Kim, S. E.; Shin, H. J.; Kim, B. T.; Kim, J. H. Brain tumor imaging with ^{99m}Tc-Tetrofosmin: comparison with ^{201}Tl, ^{99m}Tc-MIBI, and ^{18}F-fluorodeoxyglucose. *J. Neurooncol.* **2000**, *46*, 63–70.

(60) Filippi, L.; Santoni, R.; Manni, C.; Danieli, R.; Floris, R.; Schillaci, O. Imaging primary brain tumors by single-photon emission computed tomography (SPECT) with technetium-99m Sestamibi (MIBI) and Tetrofosmin. *Curr. Med. Imaging Rev.* **2005**, *1*, 61–66.

(61) Le Jeune, N.; Perek, N.; Denover, D.; Dubois, F. Influence of gluthione depletion on plasma membrane cholesterol esterification and on Tc-99m-Sestamibi and Tc-99m-Tetrofosmin uptakes: a comparative study in sensitive U87MG and multidrug-resistant MRP1 human glioma cells. *Cancer Biother. Radiopharm.* **2004**, *19*, 411–421.